Effect of Periodic Surface-Potential Variation on High-Field Tunneling in Field-Ionization Processes*

Satya P. Sharma† and George L. Schrenk
Towne School, University of Pennsylvania, Philadelphia, Pennsylvania 19104
(Received 30 October 1969; revised manuscript received 21 January 1970)

The process of field ionization is considered in this theoretical analysis as a three-dimensional rearrangement collision. The periodic potential variation in the surface region is considered to determine its effect on the field-ionization tunneling probabilities at a specific crystallographic plane. The system considered is hydrogen imaging a tungsten-type metal. A specific crystallographic plane with an interatomic spacing of π Å and an externally applied electric field of 2.3 V/Å is considered for numerical results. The analysis shows that the variation of the surface potential along the surface affects the shape of the tail of the electron wave function immediately outside the surface, and the overlap of this wave function with the wave function associated with the incoming atom leads to variation of the tunneling probability on a specific plane. It is concluded that the consideration of fine-surface-structure details does indeed lead to nonuniform tunneling probabilities on a given crystallographic plane in the field-ionization processes.

I. INTRODUCTION

The image formation in the field-ion microscope has been attributed to the tunneling of the valence electron of the incoming polarized atom into the metal under the influences of an applied electric field and surface forces. Müller[1] and others[2] have qualitatively described the process of field ionization at a metal surface on the basis of a one-dimensional model such as that shown in Fig. 1, in which the WKB approximation of quantum theory is used to calculate the probability of an electron penetrating the potential barrier into the metal. In Fig. 1, the potential energy curve of the polarized atom is shown near an idealized metal surface in an externally imposed electric field. As the atom moves closer to the metal surface, the potential barrier encountered by the valence electron of the atom becomes smaller; thus the probability of electron tunneling into the metal increases with decreasing distance between the polarized atom and the metal surface.

Using Fig. 1, the total energy of the valence electron measured from the Fermi energy and at a separation distance ρ from the metal surface may be approximated by[1,2]

$$E = eF\rho + e\Phi - eI + e^2/4\pi\epsilon_0\rho. \tag{1}$$

The first term in Eq. (1) is due to the applied electric field, which has been approximated by a field of constant strength F; the second term is due to the work function of the metal, which is denoted by Φ. The ionization energy of the free atom is denoted by I; e is the electronic charge; and ϵ_0 is the permittivity of free space. The last term in Eq. (1) results from an image potential approximation to the interaction between the valence electron and the images, in the surface of the metal, of the charges of free atom. At the low temperatures employed in field-ion microscopy, all the states below the Fermi level are occupied, and only those states whose energies are above the Fermi energy E_F are available to the tunneling electron; i.e., the energy E of the valence electron must be

$$E \geq E_F.$$

Using Eq. (1), in which the energy of the valence electron is measured from the Fermi energy, this condition can be written as

$$eF\rho_c \geq eI - e\Phi - e^2/4\pi\epsilon_0\rho_c\,, \tag{2}$$

where ρ_c is the closest point at which tunneling may occur. As the atom moves closer to the surface than this critical distance ρ_c, the barrier thickness decreases, but the energy level of the electron falls below the Fermi level of the metal and tunneling can no longer occur. Equations (1) and (2), together with Fig. 1, demonstrate that since only the energies of the valence electron, $E \geq E_F$, are permitted to the tunneling electron, ionization can occur only at distances $\rho \geq \rho_c$. The existence of this cutoff distance has been well varified experimentally.[1,3] Recent experiments by Tsong and Müller[3] on the energy distribution of ions produced in a field-ion microscope (FIM) have shown that ions are produced in a very narrow region of space just outside this critical distance; this region is called the ionization zone. Figure 2, which is based on the data obtained experimentally by Tsong and Müller thus essentially represents the tunneling

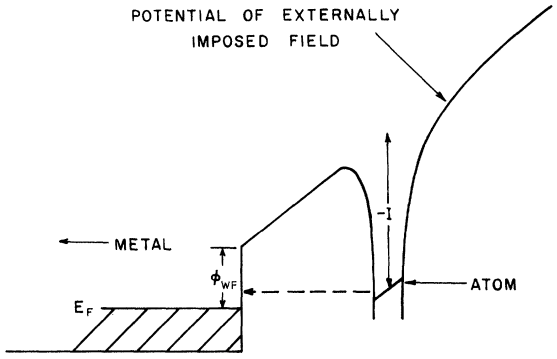

FIG. 1. One-dimensional model of field-ionization process. The valence electron of the polarized atom is shown tunneling through the potential barrier to some available state in the metal.

probability as a function of separation distance ρ between the polarized atom and the metal surface. The experimental work of Jason[4] has revealed a further structure in the energy distribution of ions. He showed the existence of secondary peaks in the energy distributions. Alferieff and Duke[5] have shown, by considering different one-dimensional models, the existence of resonance states. They thus explained the observed structure in the ionic energy distributions near nonuniform metal surfaces.

To date, one of the most refined analyses of the field-ionization process has been presented by Fonash and Schrenk.[6] Fonash and Schrenk considered the problem of the variation of tunneling probability from one crystallographic plane to another in field ionization; they treated the problem as a rearrangement collision and considered the effect of the shape of the Fermi surface of the metal on the tunneling process. Their analysis may qualitatively explain the observed variations of tunneling probability from one crystallographic plane to another. Boudreaux and Cutler[7] also treated the field-ionization process as a rearrangement collison but neglected the band-structure effects. None of these theoretical analyses, however, can explain the observed contrast on the field-ion micrographs. According to Müller,[1] the observed contrast on a specific plane in field-ion micrographs depends on the sensitivity of ionization probability to local changes in field strength. He assumed that atomic protrusions on the metal surface produce anisotropic field distribution on the metal surface, the field being higher above the lattice positions than above the trough positions. A different view concerning the cause of image formation was expressed by Brandon,[8] who considered that the field fluctuations are caused not only by atomic protrusions, but also depend on the extent to which the conduction electron cloud is pushed into the interior of the metal. Knor and Müller[9] suggested that the FIM pattern represents a projection of the places where the orbitals of the image gas particles overlap with those of surface atoms, making the electron transfer (ionization) easier. However, no known quantum-mechanical calculations have been made for any of these suggestions; the complexities in analyzing these proposals are manifold.

As mentioned before, the tunneling occurs in a narrow zone above the cutoff distance ρ_c as determined experimentally[3,4] and also predicted by simple one-dimensional considerations. In this ionization zone the field is relatively uniform, and therefore the interpretation of image contrast based on field fluctuations is not justified. The tunneling probability will, however, vary if the structure of surface potential is included in the quantum-mechanical rearrangement-collision formalism of Fonash and Schrenk.[6] The inclusion of a three-dimensional surface potential will distort the tail of the wave function outside the surface. The overlap of this wave function with the wave function associated with the electron of the incoming atom will then lead to spatial variation of the tunneling probability on a given crystallographic plane. In a narrow region near the surface, the potential varies in a plane parallel to the surface with the periodicity of metal lattice; this variation of potential must be considered in order to predict the variation in tunneling probabilities on a given crystallographic plane. Previously known theoretical calculations for the processes which take place on the surface ignore this periodicity of atomic potential at the surface and consider the potential variation as a function of the distance normal to the surface only. This analysis therefore investigates how a potential which has a periodic variation parallel to the surface, allows the ionization and/or tunneling

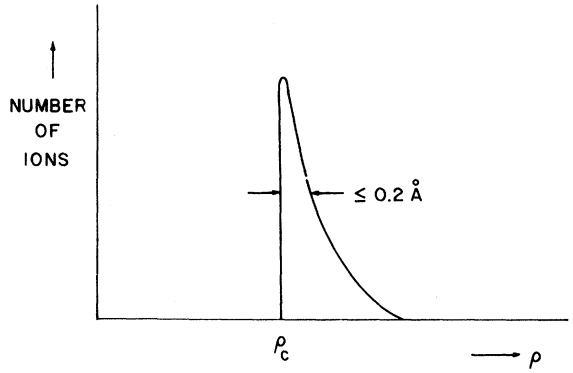

FIG. 2. Distribution of ions with the distance from the metal surface at which they were created (see Ref. 3).

probability to vary on an atomic scale on a specific surface plane, and it shows that the inclusion of surface structure may satisfactorily explain the observed contrasts on the field-ion micrographs.

This analysis treats the field ionization as a rearrangement collision. However, for reasons discussed in Sec. III, the anisotropy of the Fermi surface is not included; instead, a spherical Fermi surface is assumed. Because of the correspondence between the separation distance ρ and the energy of the tunneling electron E, it may be seen from Fig. 2 that the most probable final states for the tunneling electron are those in the energy range ΔE above the Fermi energy. This investigation considers tunneling to these most probable final states on the Fermi surface and in a shell ΔE above the Fermi surface. Furthermore, it is also discussed in Sec. III that the magnitude of ΔE need not be specified since it occurs multiplicatively in mathematical relationships. The importance of this analysis lies not only in the interpretation on an atomic scale of the intensity distribution in field-ion micrographs, but in many fields where the details of the atom-metal interaction are important, e.g., electron emission, catalysis, adsorption on metals, etc.

II. SURFACE POTENTIAL IN THE PRESENCE OF APPLIED ELECTRIC FIELD

One of the assumptions often made in the calculation of surface potentials has been that the electron density in the surface region varies only in the direction normal to the surface, that is, that the metal surface is a plane on an atomic scale. The simplest model, which has been used extensively for surface calculations, is that of noninteracting electrons in a potential well having a constant inner potential and a plane bounding surface of finite height. This model of artificial metal was named "Jellium" by Herring.[10] These over-simplified one-dimensional models of the surface-potential barrier may be the cause of some of the discrepancies between experiment and theory of processes that take place on the surface. Actually, the potential in the surface should exhibit the atomic periodicity.

Smoluchowski[11] calculated the electron density distribution due to this periodicity of core potential. He calculated the smoothing effect on the surface potential for different atomic spacings, showing that close-packed surfaces exhibit more smoothing than those with large interatomic spacing. His calculations made extensive use of the Weizsacker approximation in surface energy and are therefore numerically unreliable. Bardeen[12] made a careful study of the double layer using self-consistent solutions solutions of the Fock equations. The electronic charge distribution, obtained by solving the corresponding Fock equations, is found to be uniform throughout the crystal except in the neighborhood of the surface. Kelly[13] considered the line boundary of a two-dimensional crystal with an infinite potential well, but his two-dimensional calculations do not permit any realistic comparison with any real crystal. The most recent review on the electronic structure of clean metallic interfaces is given by Duke.[14] Smith[15] presented a self-consistent many-electron theory of electron work functions. Recently, Lang[16] considered the self-consistent properties of electron distribution at a metal surface. This is probably the first quantitative estimate of the quantum density oscillations at a metal surface. None of these analyses, however, considered the variation of potential parallel to the surface.

The many models for the potential outside a metal surface (without an imposed external field) range from the image potential model to models which consider quantum-mechanical effects. The following convenient mathematical representation of Bardeen's potential was suggested by Davis and Cutler[17]:

$$V = V_0 - (3.6/x)(1 - e^{-\lambda x}). \tag{3}$$

The parameter λ depends upon the metal considered. The value of the parameter λ in this analysis is chosen to represent tungsten and to match the calculations of Loucks and Cutler,[18] who found that this curve crosses the "surface of the metal" about $0.45V_0$, where V_0 would be the height of the barrier if a step discontinuity were assumed.[6,18] Taking V_0 at 10 eV for tungsten, the parameter λ is found to be 1.24.

Equation (3) is a good approximation in one dimension but is actually incorrect in a layer near the surface. The potential V depends also on y and z (with the periodicity of metal lattice) in this layer. The surface is actually not plane on the atomic scale. Whatever the shape of the surface happens to be, it can always be represented by a two-dimensional Fourier series of the type

$$x = \sum_{l,m=-\infty}^{\infty} A_{lm} \exp[i(lpy + mqz)], \tag{4}$$

where $p = 2\pi/d_y$, $q = 2\pi/d_z$, and d_y and d_z are the interatomic spacings in the y and z directions. x is in the direction normal to the $(HK\bar{L})$ plane of the surface. The origin for the coordinate system lies on some surface atom. The series expansion (4) is applicable to cubic and orthorhombic systems of lattices; generalization to other systems is obvious. A somewhat less general but simpler case would be to take only the two terms in the

expansion of (4). Using cosines instead of exponentials, we could then write

$$x = C_y \cos py + C_z \cos qz \quad , \tag{5}$$

where C_y and C_z are the corrugation amplitudes in the y and z directions. The Bardeen-type potential will then be modified so that the potential parallel to the surface has atomic periodicity in y and z directions and exhibits the same behavior in the x direction as the one-dimensional potential barrier. The potential function could thus be written as

$$V = V_0 - (3.6/x')(1 - e^{-\lambda x'}) , \tag{6}$$

where x' is now measured from the surface. So we could write

$$x' = x - C_y \cos py - C_z \cos qz \ . \tag{7}$$

V_0 in Eq. (6) is given by

$$V_0 = E_F + \Phi \quad , \tag{8}$$

where Φ is the work function and E_F is the Fermi energy. The total potential in the presence of applied electric field becomes

$$V_s = V + eFx' \ . \tag{9}$$

This potential represents the conditions near the surface in a qualitative manner, and will be used in this analysis.

III. REARRANGEMENT-COLLISION FORMALISM

The process of field ionizaton as it occurs in field-ion microscopy will be considered as a rearrangement collision. The final state occupied by the electron which has tunneled into the metal is taken to be a metal state. This physical picture of the valence electron occupying a metal state after tunneling has its justification if the transition time is large compared to the time an electron takes in the conduction band. Our approximate calculations reveal that this is indeed the case. The initial arrangement of the system consists of the metal tip and a polarized gas atom or molecule drifting toward the tip in the externally imposed electric field. For this initial configuration of the system, the Hamiltonian, before any interaction develops between the components of the system, is given by

$$H_i = H_N + H_A \quad , \tag{10}$$

where H_N is the Hamiltonian of the N electrons of the metal, and H_A is the Hamiltonian of an atom in the applied electric field. The state ψ_i of this initial configuration of the original system satisfies

$$(H_A + H_N)\psi_i = E_i \psi_i \quad , \tag{11}$$

where E_i is the initial energy of the system.

As the atom moves closer to the surface, the interaction potential becomes effective, which induces a transition from an initial state ψ_i to a final state ψ_f. Thus, the system is rearranged into a configuration such that the electron has tunneled from the polarized atom or molecule into the metal, and the resulting ion is being repulsed away from the tip by the externally applied electric field. The final state is described by the Hamiltonian H_f given by

$$H_f = H_{N+1} + H_B \quad , \tag{12}$$

where H_{N+1} describes the motion of $N+1$ electrons and H_B the motion of the resulting ion in the external field. H_f is the Hamiltonian of the rearranged system at large separation distance ρ, i.e., after the interaction potential of the system reduces to zero. The final state ψ_f is thus given by

$$(H_B + H_{N+1})\psi_f = E_f \psi_f \quad , \tag{13}$$

where E_f is the final energy of the system. The rearrangement of the system conserves energy; hence, this condition can be written as

$$E_i = E_f \ . \tag{14}$$

Since the Hamiltonian in Eq. (10) is the sum of two independent parts, the wave functions ψ_i are the product wave functions given by

$$\psi_i = \psi_A \Psi_N \ , \tag{15}$$

where $H_N \Psi_N = E_N \Psi_N$ (16)

and $H_A \psi_A = E_A \psi_A$. (17)

E_N and E_A are the separation constants and satisfy the relation

$$E_i = E_N + E_A \ . \tag{18}$$

Similarly, $\psi_f = \psi_B \Psi_{N+1}$, (19)

where $H_B \psi_B = E_B \psi_B$ (20)

and $H_{N+1}\Psi_{N+1} = E_{N+1}\Psi_{N+1}$. (21)

Also, $E_f = E_{N+1} + E_B$. (22)

The probability that a system initially in the state ψ_i will rearrange into a final state ψ_f may be determined from the theory of rearrangement collisions. Using the Born approximation, the expression for this probability is given by[19,20]

$$W_{if} = (2\pi T/\hbar)\, \delta(E_i - E_f) \left| \langle \psi_f | V_f | \psi_i \rangle \right|^2 . \tag{23}$$

The δ function ensures that the rearrangement of the system conserves energy. Here $\hbar$ is Plank's constant divided by 2π, and T is the time of interaction. The incoming atom moves along the lines of force to the surface, and the resulting ion moves away from the surface along these lines of force. In Sec. II, we assumed the metallic surface to be

a corrugated surface. The lines of force, in general, will be curved for a surface which is not plane. The polarized incoming atom will thus tend to move along these curved lines of force. Since the initial state ψ_i is a product wave function of ψ_A and Ψ_N as shown in (15), and the final state ψ_f is a product wave function of ψ_B and Ψ_{N+1} as shown in (19), it is quite clear, then, that the probability of tunneling depends upon the path of the incoming atom and the path of resulting ion away from the surface. To formulate a proper expression for this probability of tunneling, we should find the equations of lines of force for a corrugated surface. The solution of this problem is quite difficult; hence, we resort to an approximation to see how the lines of force behave near a corrugated surface. We considered the space included between two of the equipotential surfaces, one of which consists of an undulating surface, while the other corresponds to a large value of potential and may be considered as approximately plane. This problem has been considered by Maxwell[21] in his treatise on electricity and magnetism. It is shown in Fig. 3 that the equipotential surfaces between an undulating surface (which we took as the metallic surface) and a plane surface at infinity soon reduces to plane surfaces at about 3–4 Å from the surface. It can also be shown easily that for small corrugations the lines of force also become straight lines at about 3 Å from the surface. Since the atom never reaches the surface closer than the cutoff distance imposed by the Pauli principle, which is of the order of about 3.5 Å for the tungsten-hydrogen system under consideration here, it is then a very good approximation to consider that the atom approaches the surface normal to the plane $x=0$, i.e., normal to the crystallographic plane (HKL). Thus, the incoming atom approaches the surface normal to plane (HKL) and, under the influence of the applied electric field, the resulting ion moves away from the surface normal to plane (HKL). The time of interaction T in Eq. (23) could then be considered a constant.

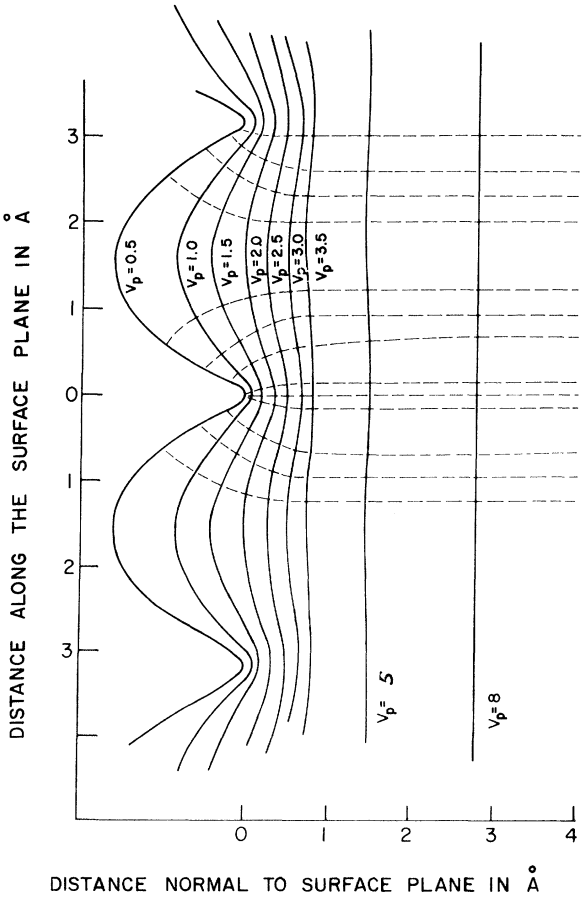

FIG. 3. Equipotentials and lines of force between an undulating boundary and a plane at infinity. Firm lines represent the equipotentials, and dotted lines, the lines of force. This figure has been obtained by considering an infinite series of planes parallel to xz at distances equal to the interatomic distance of π Å and all cut off by the plane of yz so that they extend only on the negative side of yz plane.

Equation (23) gives the probability that the system rearranges itself such that the electron of the incoming atom occupies a $\vec{k}$ state over the Fermi surface. The total probability of tunneling will involve a sum of such expressions over the allowed $\vec{k}$ values, that is, a sum over all allowed final states of the system. The number of $\vec{k}$ states in a volume of $\vec{k}$ space with energies lying between E and $E+\Delta E$ and whose base is ΔS, an element of area on a constant energy surface, is given by[22]

$$\Delta N(\vec{k}) = \frac{\Omega}{(2\pi)^3} \frac{1}{|\nabla E|} \Delta S \, \Delta E \ , \qquad (24)$$

where Ω is the volume of the metal. Therefore, using Eqs. (23) and (24) we could write the total probability of tunneling at a surface plane of a given crystallographic orientation (HKL) as

$$P_{HKL} = \frac{\Omega T}{2\pi h} \delta(E_i - E_f) \int_k \frac{|\langle \psi_f | V_f | \psi_i \rangle|^2}{|\nabla E|} \, dS \, dE \ . \qquad (25)$$

The range of integration in Eq. (25) must be over the volume in the Brillouin zone which contains allowed final $\vec{k}$ states for the electron which has tunneled into the metal. From our previous discussion in Sec. I, it is known that these allowed $\vec{k}$ states have energies $E \geq E_F$. Therefore, dE ranges over energies greater than E_F the Fermi energy. It will be assumed in what follows that the Fermi surface of the metal is a sphere. This is assumed because we are more interested in find-

ing the effect of surface structure in the process of field ionization than the effect of actual band structure of the metal. Fonash and Schrenk[6] considered this band structure and predicted the variation of tunneling probability for different crystallographic planes qualitatively. This analysis will concentrate on predicting the variation in tunneling probability on a specific plane; band-structure effects cannot account for this. The assumption of a spherical Fermi surface is thus physically plausible for the problem under consideration. To minimize the computational difficulties, a further simplification is made. In Sec. I, it was seen that those states whose energies lie in a range ΔE above the Fermi surface are the most probable final states. The inclusion of structure in the energy distribution of ions, revealed by Jason[4] and Alferieff and Duke,[5] will not effect the justification of this assumption. In this analysis, we consider the tunneling to only these most probable final states. There is no need to specify the magnitude of ΔE since it occurs multiplicatively in the succeeding equations. It must, however, be added that ΔE is considered to be large enough to include these most probable final states and small enough so that the mathematical statements may have some meaning. Our approach, therefore, closely resembles the approach taken by Fonash and Schrenk.[6] The probability that the valence electron tunnels into one of these most probable final states will therefore be given by

$$\Delta P=\frac{\Omega T}{2\pi h}\,\delta(E_i-E_f)\iint_S \frac{|\langle\psi_f|V_f|\psi_i\rangle|^2}{|\nabla E|}\,dS\,\Delta E\ , \tag{26}$$

where dS ranges over that part of the Fermi surface which projects onto the surface plane of tunneling.

The concept of cutoff distance ρ_c will have to be modified for a corrugated surface. The significance of ρ_c hinges on the definition of the surface.[8] The equipotential surfaces near a corrugated boundary quickly become plane at about 3–4 Å from the surface. ρ_c is the distance of the ionization zone from the edge of the Fermi sea. For energy balance of the valence electron, the potential difference between a plane surface at the cutoff distance and the corrugated boundary will be needed. Thus, the cutoff distance itself will move in towards the ion cores.[8] A very reasonable assumption will be that the cutoff distance ρ_c will be measured from the corrugated surface.

To evaluate the matrix element in (26), functional forms are required for ψ_A, ψ_B, Ψ_N, Ψ_{N+1}, and V_f. The function V_f is the interaction potential energy of the ion with the metal tip. For the small separation distance, V_f is clearly a function of the coordinates of the $N+1$ electrons in the metal tip and the coordinates of remaining electrons and nucleus of the ion. For large separation distances, this function may be approximated by the interaction of the various charges of the ion with their images in the tip. Choosing the free gas to by hydrogen,[6]

$$V_f=-e^2/4\rho\ , \tag{27}$$

where ρ is the separation distance. We now consider the initial and final states of the electrons in the metal. Ψ_N describes the wave function of the original N electrons of the metal. Taking the Hamiltonian H_N as the sum of N single-electron Hamiltonians of the Hartree-Fock form, i.e.,

$$H_N=\sum_{i=1}^{N} H_i\ , \tag{28}$$

the Ψ_N is then of the form

$$\Psi_N=\textstyle\sum_P(-1)^p P\prod_n\psi_n, \tag{29}$$

where P represents the permutation operator. The state $\{\psi_n\}$ of single-electron states is assumed to be normalized.

The wave function Ψ_{N+1} represents the motion of $N+1$ electrons in the metal; the Hamiltonian H_{N+1} is the Hamiltonian of the metal with $N+1$ electrons in the metal; as in the case of H_N it will be assumed that H_{N+1} can be written as the sum of $N+1$ single-electron Hamiltonians of Hartree-Fock form, i.e.,

$$H_{N+1}=\sum_{i=1}^{N+1} H_i\ . \tag{30}$$

The state Ψ_{N+1} is thus of the form

$$\Psi_{N+1}=\textstyle\sum_P(-1)^p P[\psi(\vec{k})\prod_n\psi_n]\ . \tag{31}$$

The state $\psi(\vec{k})$ is the $\vec{k}$ state which the electron occupies after tunneling into the metal.

The Hamiltonian H_A for the hydrogen atom can be written as

$$H_A=-\frac{\hbar^2}{2M}\nabla_n^2-\frac{\hbar^2}{2M}\nabla_e^2-\frac{e^2}{4\pi\epsilon_0|r_n-r_e|}-eF\rho+eFx\ . \tag{32}$$

The subscript n refers to the nucleus and e to the electron. M and m are the masses of the proton and the electron, respectively, and ϵ_0 is the permittivity of free space. r_n and r_e are the positions of nucleus and electron, respectively. ρ and x are the components of position vectors normal to the surface. The general motion as described by Eq. (32) can be represented as an orbital motion of the particles about their common center of mass plus a uniform linear motion of this center of mass. Thus, Eq. (32) is separable in a coordinate system which uses the center-of-mass

vector ρ and the relative coordinate of the two particles R as the independent variables. Such a separation of the Hamiltonian operator into independent parts always leads to eigenfunctions which are a product of separate eigenfunctions. Thus,

$$\psi_A = \psi_{\text{c.m.}}\,\psi_{\text{rel}}, \tag{33}$$

where $$[-\hbar^2/2(m+M)]\,\nabla_\rho^2\,\psi_{\text{c.m.}} = E_{\text{c.m.}}\,\psi_{\text{c.m.}} \tag{34}$$

and

$$-\frac{\hbar^2}{2m_r}\,\nabla_R^2\,\psi_{\text{rel}} - \frac{e^2}{4\pi\epsilon_0|R|}\,\psi_{\text{rel}} - eFX\,\psi_{\text{rel}} = E_{\text{rel}}\,\psi_{\text{rel}}\ , \tag{35}$$

where $X = \rho - x$, and $E_{\text{c.m.}}$ and E_{rel} are the separation constants. In the above equations $(m+M)$ and m_r could effectively be replaced by M and m, respectively, because the mass of a proton is 1836 times that of an electron. Equation (34) gives us

$$\psi_{\text{c.m.}} = e^{-i\delta\rho}\ , \tag{36}$$

where $$\delta = (2ME_{\text{c.m.}}/\hbar^2)^{1/2}\ . \tag{37}$$

In cgs units $E_{\text{c.m.}}$ is $\frac{1}{2}\omega F^2$, where ω is the polarizability of hydrogen.

In the absence of an external field, Eq. (35) describes the motion of an electron about its nucleus. The soltuion to the equation in the absence of the external field is given by $\exp(R/a_0)$, where a_0 is the Bohr radius. The effect of introducing the external field is to perturb this state. The solution is thus

$$\psi_{\text{rel}} = N_0 e^{-R/a_0}(1+\alpha X)\ , \tag{38}$$

where N_0 is the normalization constant, and α is the polarization parameter. An approximation to α is obtained by variation techniques. These calculations yield[23]

$$\alpha = F/I\ . \tag{39}$$

The state ψ_A is then simply

$$\psi_A = N_A e^{-R/a_0}[1+(F/I)X]e^{-i\delta\rho}\ . \tag{40}$$

The Schrödinger equation for the hydrogen ion can be written as[6]

$$(-\hbar^2/2M)\nabla_\rho^2\psi_B - eF\rho\psi_B = E_B\psi_B\ . \tag{41}$$

Following Fonash,[6] E_B is the sum of the kinetic energy of the atom and the potential energy of the ion in the external field at the point of ionization ρ_c. Thus,

$$(-\hbar^2/2M)\nabla_\rho^2\psi_B - eF\rho\psi_B = (E_D - eF\rho_c)\psi_B\ , \tag{42}$$

where E_D is the energy of the atom. With the following change of independent variable,

$$\xi = (2MeF/\hbar^2)^{1/3}(\rho - \rho_c + E_D/eF)\ , \tag{43}$$

the solution to ψ_B, which represents the wave moving away from the surface, is

$$\psi_B = \mathrm{Ai}(-\xi) - i\,\mathrm{Bi}(-\xi)\ . \tag{44}$$

ψ_i may explicitly be written as[6]

$$\psi_i = N_i e^{-i\delta\rho\sum_P(-1)^p} \times P\{\textstyle\prod_n \psi_n e^{-R/a_0}[1+(F/I)X]\}\ , \tag{45}$$

and, similarly, the final rearranged state ψ_f may be written as[6]

$$\psi_f = N_f[\mathrm{Ai}(-\xi) - i\mathrm{Bi}(-\xi)]\Psi_{N+1}\ , \tag{46}$$

where N_i and N_f are the normalization factors.

It will be shown later that only the functional form of the state $\psi(\vec{k})$, i.e., the state the electron had occupied after tunneling into the metal, is needed to evaluate the matrix element in the expression for total probability of tunneling; expressions for the N states below the Fermi level are not required in the evaluation of total probability of tunneling. Since the major contribution to the total probability of tunneling comes from the tail of the wave function outside the metal surface, for convenience the Bloch wave inside the metal may be approximated by a plane wave

$$\psi'(\vec{k}) = e^{ik_x x}e^{ik_y y}e^{ik_z z}\ . \tag{47}$$

Equation (47) represents a plane wave approximation to some $\vec{k}$ state. k_x, k_y, and k_z satisfy the relation

$$k_x^2 + k_y^2 + k_z^2 = 2mE_f/\hbar^2\ . \tag{48}$$

The wave strikes the surface of the metal at some angle γ. There will be waves reflected back into the metal and the tails outside.

The equation of the reflecting surface is given by

$$x = C_y\cos py + C_z\cos qz\ . \tag{49}$$

If the surface were plane, there would only be a regularly reflected wave into the metal, but because of the presence of corrugation in the reflecting surface the terms involving $\cos mpy$ and $\cos nqz$ (m and n integers) will also be present in the reflected waves. The coefficient of the incident wave may be taken as unity without any loss of generality. Using the exponentials instead of cos and sin, the $\psi(\vec{k})$ for $x' < 0$ (i.e., inside the metal) could be written as

$$\psi(\vec{k}) = e^{ik_x x}e^{ik_y y}e^{ik_z z} + \sum_{r,l} A_{rl}e^{-ik_x x}e^{ik'_y y}e^{ik'_z z}\ . \tag{50}$$

$\psi(\vec{k})$ for the region inside the metal as given by Eq. (50) contains all the reflected waves with momentum $\vec{k}'$ (i.e., k'_x, k'_y, k'_z). However, all the reflected waves should still satisfy the condition

$$k_x'^2 + k_y'^2 + k_z'^2 = 2mE_f/\hbar^2 \quad . \tag{51}$$

The observable $\psi^*\psi$ should exhibit the periodicity with the period of the lattice. This condition leads to

$$k_y' = k_y \pm rp \tag{52}$$

and $$k_z' = k_z \pm lq \quad . \tag{53}$$

Thus, the electron wave function inside the metal will be

$$\psi(\vec{k}) = e^{ik_y y} e^{ik_z z}\left(e^{ik_x x} + \sum_{r,l}^{\infty} A_{rl} e^{-ik_{xrl} x} e^{irpy} e^{ilqz}\right), \tag{54}$$

where $$k_{xrl}^2 = (2mE_f/\hbar^2) - (k_y + rp)^2 - (k_z + lq)^2 \ , \tag{55}$$

and r and l could take all positive and negative values, as well as zero.

The electron wave function for the state $\psi(\vec{k})$ inside the metal near the surface of discontinuity has to be matched with the wave function outside the metal. Inside the metal we have a perfect periodic crystal. The incident wave is, in fact, a Bloch wave, and the above wave function based on the free-electron theory will be somewhat modified. The primary effect of the periodic structure inside the metal will be to introduce the band gaps. We will exclude these energy gaps from our formulation. It will be assumed that the plane at which tunneling occurs is of infinite extent. This is justified since the wavelength of an electron at the Fermi level is of the order of 2–3 Å. The tunneling electron thus sees the plane as having infinte extent. We now need to write the Schrödinger equation for an electron outside the metal. In Sec. II we developed an expression for the potential function outside the metal surface. Therefore, outside the metal, for some $\vec{k}$ state on the Fermi surface, we may write

$$\frac{-\hbar^2}{2m}\nabla^2\psi(\vec{k}) + \left(V_0 + eFx' - \frac{3.6}{x^1}(1 - e^{-\lambda x'})\right) \times \psi(\vec{k}) = E_f\psi(\vec{k}) \ , \tag{56}$$

where x' is measured from the surface and is given by

$$x' = x - C_y \cos py - C_z \cos qz \quad . \tag{57}$$

The solutions of interest for $\psi(\vec{k})$ are the states at the Fermi level, and so $E_f = E_F$. V_0 in Eq. (56) is given by $V_0 = \Phi + E_F$. To solve Eq. (56), some approximations are necessitated. The circled points in Fig. 4 represent a plot of

$$\Phi - (3.6/x')(1 - e^{-1.24x'}) \tag{58}$$

at some given values of y and z. It is seen from Fig. 4 that in the region outside the metal surface the potential may be approximated by a linear potential of the form

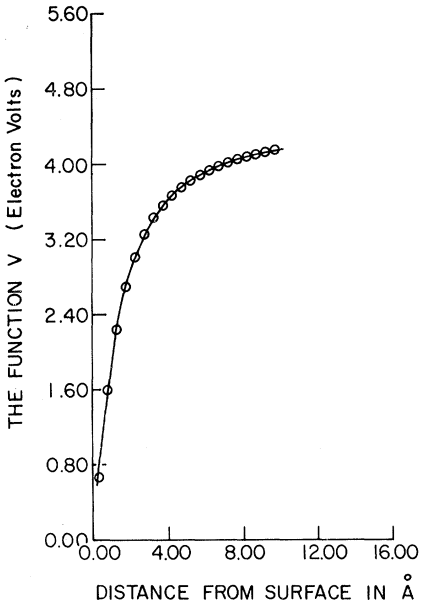

FIG. 4. Plot of surface potential in the absence of applied electric field.

$$V_S = A + Bx' + Fx' + E_F. \tag{59}$$

Using this potential, the Schrödinger equation reduces to

$$\nabla^2\psi(\vec{k}) - (2m/\hbar^2)[A + (B+F) \times (x - C_y \cos py - C_z \cos qz)]\,\psi(\vec{k}) = 0. \tag{60}$$

The solution to Eq. (60), as developed in the Appendix, is given by

$$\psi(\vec{k}) = \sum_{r,s}^{\infty} F_{rs} \exp[i(\alpha_y + r)py]\, e^{[i(\alpha_z + s)qz]} \times \left(\sum_{l,m}^{\infty} B_{lm}(r,s) \exp[i(lpy + mqz)]\ \mathrm{Ai}(\eta_{rs})\right). \tag{61}$$

As shown in the Appendix, α_y and α_z are equal to k_y/p and k_z/q and Ai is the Airy function. The constants F_{rs} and B_{lm} are determined in the Appendix. The F_{rs}'s are obtained by matching the wave function and its normal derivative across the surface; and

$$\eta_{rs} = (2m/\hbar^2)^{1/3}(B+F)^{-2/3}\{A + (B+F)x + (\hbar^2 p^2/2m) \times [(\alpha_y + r)^2 + f_y(r)] + (\hbar^2 q^2/2m)[(\alpha_z + s)^2 + f_z(s)]\}. \tag{62}$$

f_y and f_z have been explained in the Appendix. If, instead of Eq. (5), a general expansion of the type given in Eq. (4) is assumed to represent the surface, the potential function in Eq. (60) would contain an infinite two-dimensional Fourier series in y and z directions; i.e., the potential function would be of the form

$$V_s = A + (B+F)\left(x - \sum_{l,m} A_{lm} e^{i(lpy + mqz)}\right) + E_F. \tag{63}$$

The generalization of Hill's arguments[24] shows that a solution of the Schrödinger equation using the general potential function given above will be of the form $\psi(y, z)\psi(x)$, and $\psi(y, z)$ will be given by

$$\psi(y, z) = N' e^{i(\beta_y p y + \beta_z q z)} \left(\sum_{l,m}^{\infty} D_{lm} e^{ilpy} e^{imqz} \right), \quad (64)$$

where the relations between β's are given by the equation

$$S(\beta_y, \beta_z, p, q) = S(W_y^{1/2}, W_z^{1/2}, p, q) \square(0, 0) \quad (65)$$

and where $\square(0, 0)$ is a determinant similar to $\square(0)$ of the Appendix. As shown by Morse, [24] for a two-dimensional case $S(y, z, p, q)$ is the product of the elliptic functions $H(y+iz) \times H(y-iz)$, where the periods of these functions are $\frac{1}{2}p$ and $\frac{1}{2}q$. For the one-dimensional case, $s(y, p)$ is $\sin^2(\pi y/p)$, as given in the Appendix. The D's are given by equations similar to the equations for the B's in the Appendix, namely,

$$[(\beta_y + rp)^2 + (\beta_z + sq)^2 - W_y - W_z] D_{r,s} + \sum_{l,m} A'_{lm} D_{r-l, s-m} = 0. \quad (66)$$

For calculating the matrix element, it will be assumed that only the two terms in the expansion (4) are dominant; hence, Eq. (5) represents the surface to a good accuracy. The implications of this assumption are obvious: The potential function will have a simpler form and make the problem easier to solve. With these considerations in mind, we will take the solution (61) to be a reasonably good approximation to the wave function outside the surface. It will be seen later that it is the wave function immediately near the surface that contributes the maximum to the expression in (26). A more accurate solution would result by taking the potential function to be an infinite Fourier series as discussed above, but the added complexity will not alter the quantitative results by any appreciable degree.

Using (45), (46), and (27) the expression for the matrix element to be evaluated in (26) can be written as

$$T_m = N \int_{\rho_c}^{\infty} \{e^{-i\delta\rho} [\mathrm{Ai}(-\xi) + i\,\mathrm{Bi}(-\xi)]/\rho\} \times \int\int\int_{V_{N+1}} \{\textstyle\sum_P (-1)^p P[\psi^*(\vec{k}) \prod_n \psi_n^*]\} \times \{\textstyle\sum_P (-1)^p P[e^{-R/a_0}(1 + FX/I) \prod_n \psi_n]\}\, dV_{N+1}\, d\rho, \quad (67)$$

where N incorporates all the constants which are independent of the plane of tunneling. The lower limit on ρ integration is ρ_c, because, as discussed in Sec. I, the energy conditions as expressed by the Dirac δ function in Eq. (26) cannot be met by[6,7]

$$\rho < \rho_c.$$

The integration over dV_{N+1} is limited to the region outside the surface.[7] The set $\{\psi_n\}$ depends only upon the internal coordinates of the N electrons of the metal; this set is assumed to be normalized. The above expression thus simplifies to

$$T_m = N \int_{\rho_c}^{\infty} (e^{-i\delta\rho}/\rho) [\mathrm{Ai}(-\xi) + i\,\mathrm{Bi}(-\xi)] \times \left\{ \int_{-\infty}^{\infty} \int_{-\infty}^{\infty} \int_{0}^{\infty} \psi^*(\vec{k}) e^{-R/a_0} (1 + FX/I)\, dy\, dz\, dx' \right\} d\rho. \quad (68)$$

The term in curly brackets in Eq. (68) is just the overlap integral of the tail of the final electron state in the metal with the perturbed $1s$ state of hydrogen atom for various values of the separation distance ρ. Let this be represented by λ_0. By using the definition

$$\sigma(\vec{k}) = \int_{\rho_c}^{\infty} (e^{-i\delta\rho}/\rho) [\mathrm{Ai}(-\xi) + i\,\mathrm{Bi}(-\xi)] \lambda_0(\rho, \vec{k})\, d\rho, \quad (69)$$

Eq. (26) may be written as

$$\Delta P_{HKL} = \mu \int_S [\,|\sigma(\vec{k})|^2 / |\nabla_K E|\,]\, dS\, \Delta E, \quad (70)$$

where μ absorbs all the constants which are independent of the plane of tunneling and dS ranges over that part of the Fermi surface which projects onto the surface plane of tunneling. In other words, the integration in (70) is performed over states that represent waves crossing the surface plane (HKL). As pointed out before, the Fermi surface is assumed to be spherical. The justification for assuming the spherical Fermi surface, as explained before, comes from the fact that we want to look at the variation of tunneling probability on a specific plane, and band-structure effects will not predict these variations. The total tunneling current density J_{HKL} at some point of a surface plane is the product of Eq. (70), integrated over all energies $E \geq E_F$ and the supply function W_s, where W_s is the number of hydrogen atoms arriving at the surface plane per unit of time and area. W_s is assumed to be constant for all points of the surface plane in this analysis.

IV. EVALUATION AND RESULTS

For evaluating the expression for ΔP_{HKL} at different points of the surface, it will be convenient to define $\psi(\vec{k})$ in a new coordinate system defined in the corrugated surface. Let the new origin have the coordinates $(C_y \cos(p\beta_1 d_y) + C_z \cos(q\beta_2 d_z),\ \beta_1 d_y,\ \beta_2 d_z)$ with respect to the old coordinate system; the parameters β_1 and β_2 represent the translation along the y and z axes; d_y and d_z are the interatomic spacing in the y and z directions. If the expression for $\psi(\vec{k})$ in this new coordinate system is introduced into the matrix element we will get

$$T_m = \text{const} \times 2\pi \int_{\rho_c}^{\infty} (e^{-i\delta\rho}/\rho)[\mathrm{Ai}(-\xi) + i\,\mathrm{Bi}(-\xi)] \Big[\int_{-\infty}^{\infty}\int_{-\infty}^{\infty}\int_{0}^{\infty} \Big(\sum_{r,s=-\infty}^{\infty} F_{rs}^{*} \sum_{l,m=-\infty}^{\infty} B_{lm}(r,s)$$

$$\times \cos[(\alpha_y + r + l)py] \cos[(\alpha_z + s + m)qz] \exp[-i(\alpha_y + r + l)p\beta_1 d_y]$$

$$\times \exp[-i(\alpha_z + s + m)q\beta_2 d_z] \,\mathrm{Ai}(\eta'_{rs}) \Big) [1 + (F/I)(\rho - x)] \exp(-\{[(\rho - x)^2 + y^2 + z^2]^{1/2}/a_0\}) \, dy\, dz\, dx \Big] d\rho , \quad (71)$$

where $$\eta'_{rs} = (2m/\hbar^2)^{1/3}(B+F)^{-2/3}\{A + (B+F)\,[x + C_y \cos(p\beta_1 d_y) + C_z \cos(q\beta_2 d_z)]$$

$$+ (\hbar^2 p^2/2m)[(\alpha_y + r)^2 + f_y(\alpha_y, r)] + (\hbar^2 q^2/2m)[(\alpha_z + s)^2 + f_z(\alpha_z, s)]\} . \quad (72)$$

Introducing a new set of coordinates

$$x = \rho - R\cos\theta , \quad y = R\sin\theta\cos\phi , \quad z = R\sin\theta\sin\phi , \quad (73)$$

and integrating over ϕ analytically, we get

$$T_m = 2\pi\,\text{const} \times \int_{\rho_c}^{\infty} (e^{-i\delta\rho}/\rho)[\mathrm{Ai}(-\xi) + i\,\mathrm{Bi}(-\xi)] \Big[\int_{0}^{r_c} \int_{0}^{\pi} \Big(\sum_{r,s} F_{rs}^{*} \sum_{l,m} B_{lm}(r,s) J_0(u) \exp\{-i[(\alpha_y + r + l)p\beta_1 d_y]\}$$

$$\times \exp\{-i[(\alpha_z + s + m)q\beta_2 d_z]\} \,\mathrm{Ai}[\eta'_{rs}(\rho - R\cos\theta)] \Big) [1 + (F/I)R\cos\theta] \, e^{-R/a_0} R^2 \sin\theta \, d\theta \, dR \Big] d\rho , \quad (74)$$

where J_0 is the zero-order Bessel function and u is given by

$$u = [(\alpha_y + r + l)^2 p^2 + (\alpha_z + s + m)^2 q^2]^{1/2} R \sin\theta . \quad (75)$$

For any given ρ in the range of interest, it was determined numerically that the principal contribution to the overlap λ_0 comes from the region outside the metal surface. This permitted the assumption that the hydrogenic wave function is zero at distances greater than 3.52 Å from the atom; thus, the limit r_c in Eq. (74) is 3.52 Å. This assumption has also been made by other authors[6,7] and is justified. The overlap is also a function of the position on the surface, i.e., it is different at different points on the surface. A computer program was written to evaluate the overlap λ_0 for a given $\vec{k}$ state for various values of ρ at various points of the surface by choosing different values of β_1 and β_2. A work function of 4.5 eV, a Fermi energy of 5.5 eV, and a field strength F of 2.3 V/Å were used in this analysis. This value of field strength is typical of the magnitudes used in field-ion microscopy. The corrugation amplitudes C_y and C_z were taken to be $\frac{1}{16}\pi$ Å in each of the y and z directions. These values of corrugation amplitudes are reasonable; in fact, the correct corrugation amplitudes should be determined from microscopic considerations. The distribution of charge in the surface region should be constructed in detail, and considerations similar to those of Smoluchowski[11] and Kelly[13] should be employed to obtain the details about the corrugated surface. An alternative approach will be to calculate the surface energy for a corrugated surface and then to minimize the total surface energy with respect to the surface corrugation parameters in order to obtain the actual corrugated surface. This, however, was not done, and corrugation amplitudes of $\frac{1}{16}\pi$ Å in each of the y and z directions were assumed for numerical calculations. This was felt to be quite reasonable to show the effect of corrugation on tunneling probabilities on a surface plane. Because of the excessive amount of computer time needed for evaluating the overlap λ_0 for each value of corrugation amplitude, the numerical calculations were not repeated for many different values of C_y and C_z. The numerical results will, however, be quite sensitive to corrugation amplitudes because, as explained in the Appendix, the higher the corrugation, the greater will be the distortion of the wave function near the surface. Thus, the effect on the overlap λ_0 and hence on ΔP_{HKL} will be quite appreciable. For a given $\vec{k}$ value, the overlap was calculated for 20 values of ρ at intervals of 0.1 Å. For each $\vec{k}$ value, it required about 25 min on the IBM 360/75 computer to evaluate λ_0. These values of λ_0 were then tabulated for the 20 values of ρ for a given $\vec{k}$. The values of ρ were so chosen that efficient use would be made of a four-point Lagrangian interpolation subroutine to obtain the overlap at any value of ρ for a given $\vec{k}$ value. This interpolation scheme is necessary since, for a given $\vec{k}$, λ_0 should be known for large values of ρ to perform the integration for $\sigma(\vec{k})$. To evaluate the expression for $\sigma(\vec{k})$ in Eq.

(69), Simpson's rule is used. The intervals in Simpson's rule are so chosen that they are small compared to the wavelength of the exponential function in Eq. (69). The expression ΔP_{HKL} as given in Eq. (70) was then evaluated for a spherical Fermi surface. The results are presented in Table I for various points of a surface plane of interatomic spacing π Å each in the y and z directions.

V. CONCLUSION

The variation of potential parallel to the surface leads to the generalized Mathieu solutions in the y and z directions (along the surface) and the Airy functions in the x direction (normal to the surface) for the tail of the wave function outside the metal surface. The expression for ΔP_{HKL} at different points on a given plane was then evaluated by introducing this tail of the wave function into the rearrangement-collision formalism. This analysis has shown that a consideration of surface-structure details, i.e., the potential variation in the surface region, can lead to variation of tunneling probability on a given surface. Since the image in the field-ion microscope is produced by the ion current, this analysis can predict the bright spots and the surrounding dark regions on the field-ion micrographs.[25] The results presented are only for a plane whose interatomic spacing in y and z directions is π Å, and by assuming the corrugation amplitudes of $\frac{1}{16}\pi$ Å in the y and z directions, each.

TABLE I. The relative values of $\Delta P_{HKL}/\mu\Delta E$ at various points of the crystallographic plane. The origin of the coordinate system is located on some atom. d_y and d_z are the interatomic spacings in y and z directions, which are taken to be π Å each. These results are for corrugation amplitudes of $\frac{1}{16}\pi$ Å each in y and z directions. These results have not been normalized.

y	z	Tunneling probability
0.0	0.0	1.844
0.0	$\frac{1}{4}d_z$	1.794
0.0	$\frac{1}{2}d_z$	1.742
0.0	$\frac{3}{4}d_z$	1.794
$\frac{1}{4}d_y$	0.0	1.794
$\frac{1}{4}d_y$	$\frac{1}{4}d_z$	1.745
$\frac{1}{4}d_y$	$\frac{1}{2}d_z$	1.707
$\frac{1}{4}d_y$	$\frac{3}{4}d_z$	1.745
$\frac{1}{2}d_y$	0.0	1.742
$\frac{1}{2}d_y$	$\frac{1}{4}d_z$	1.684
$\frac{1}{2}d_y$	$\frac{1}{2}d_z$	1.650
$\frac{1}{2}d_y$	$\frac{3}{4}d_z$	1.684
$\frac{3}{4}d_y$	0.0	1.794
$\frac{3}{4}d_y$	$\frac{1}{4}d_z$	1.745
$\frac{3}{4}d_y$	$\frac{1}{2}d_z$	1.707
$\frac{3}{4}d_y$	$\frac{3}{4}d_z$	1.745

Identical calculations can be performed for other surface planes. The numbers in Table I represent the relative magnitudes of $\Delta P_{HKL}/(\mu\Delta E)$ at different points of a given plane. The results show that the probability of tunneling is maximum above a surface atom and is minimum at the diagonal interaction of the rectangle, the vertices of which represent the location of atoms in the surface. The electron distribution near the surface of the metal has been determined for the auxiliary potential developed in Sec. II. This potential represents to some degree the conditions near the surface. Electron density in the surface region should reflect to some degree the periodicity of the atomic potential. It was thus shown that the variation of the local surface potential parallel to the surface affects the tail of the wave function immediately outside the surface. The overlap of this wave function with the electron wave function associated with the incident atom leads to a variation of tunneling probability in a region where the actual potential is reasonably constant. The Pauli exclusion principle restricts the tunneling to a narrow zone sufficiently far from the surface where the isopotential surfaces are approximately planes.

This analysis did not consider the anisotropy of the Fermi surface and the anisotropy of the work function. Both of these could be included into the analysis with added complexities. However, the anisotropies of the Fermi surface and work function are important when comparing the tunneling probabilities between different surface planes. We also presented a solution to a complicated boundary given by infinite series in the y and z directions. We then considered a special case of taking the two terms as the dominant terms in that expansion. In a general case, the process of matching the wave function and its derivative on a complicated boundary is quite difficult. The results of this analysis demonstrate that the inclusion of complex surface structure does indeed lead to nonuniform tunneling probabilities on a surface plane and is therefore important when details near the surface have to be examined.

APPENDIX

As shown in Sec. III, the wave function $\psi(\vec{k})$ is a solution to the equation

$$\nabla^2\psi - (2m/\hbar^2)[A + B(x - C_y\cos py - C_z\cos qz) + F(x - C_y\cos py - C_z\cos qz)]\psi = 0 . \quad \text{(A1)}$$

The constants appearing in the resulting solution must be obtained by matching the wave function and its normal derivative across the surface:

$$x = C_y\cos py + C_z\cos qz . \quad \text{(A2)}$$

Because the Hamiltonian in (A1) can be written as the sum of three parts, the wave function will be a product wave function of the form

$$\psi(\vec{k}) = \psi_x \psi_y \psi_z \,, \tag{A3}$$

where ψ_x, ψ_y, and ψ_z are the solutions of the following equations, respectively:

$$d_z \psi_x/dx^2 - (2m/\hbar^2)[A + (B+F)x + a_x]\psi_x = 0 \,, \tag{A4}$$

$$d_2 \psi_y/d\xi_y^2 + [W_y + A_y e^{i\xi_y} + A_y e^{-i\xi_y}]\psi_y = 0 \,, \tag{A5}$$

and

$$d_2\psi_z/d\xi_z^2 + [W_z + A_z e^{i\xi_z} + A_z e^{-i\xi_z}]\psi_z = 0 \,, \tag{A6}$$

where ξ_y and ξ_z are given by

$$\xi_y = py \tag{A7}$$

and

$$\xi_z = qz \,. \tag{A8}$$

$(2m/\hbar^2)a_x$, $W_y p^2$, and $W_z q^2$ are the separation constants in x, y, and z directions which satisfy the condition that

$$a_x = W_y \hbar^2 p^2/2m + W_z \hbar^2 q^2/2m \,. \tag{A9}$$

A_y and A_z stand for

$$A_y = (m/\hbar^2 p^2)(B+F)\,C_y \tag{A10}$$

and

$$A_z = (m/\hbar^2 q^2)(B+F)\,C_z \,. \tag{A11}$$

The solutions to (A5) and (A6) are the generalized Mathieu functions as discussed in the literature[24,26]:

$$\psi_y = N_y e^{i\alpha_y \xi_y} \sum_{r=-\infty}^{r=\infty} b_{y,r}(\alpha_y)\, e^{ir\xi_y} \tag{A12}$$

and

$$\psi_z = N_z e^{i\alpha_z \xi_z} \sum_{l=-\infty}^{\infty} b_{z,l}(\alpha_z)\, e^{il\xi_z} \,. \tag{A13}$$

N_y and N_z are the normalization constants in the y and z directions, respectively. Combining (A12) and (A13) we can write the solution in the y-z directions as

$$\psi_y \psi_z = N_{yz} e^{i(\alpha_y py + \alpha_z qz)} \sum_{r,s=-\infty}^{\infty} B_{rs}(\alpha_y, \alpha_z)\, e^{i(rpy + sqz)} \,, \tag{A14}$$

where

$$B_{rs}(\alpha_y, \alpha_z) = b_r(\alpha_y)\, b_s(\alpha_z) \,. \tag{A15}$$

The expressions (A12) and (A13) are of natural form, that of a free electron (whose direction cosines are proportional to α_y and α_z, respectively) multiplied by a function representing the distortion of a wave function due to the periodic variation of the potential function.

The relations between α's are given by the equations

$$\sin^2 \pi\alpha_z = \sin^2 \pi (W_z)^{1/2} \square(0) \tag{A16}$$

and

$$\sin^2 \pi\alpha_y = \sin^2 \pi (W_y)^{1/2} \square(0) \,,$$

where $\square(0)$ is the infinite Hill determinant, as shown in the literature. The procedure for calculating α's and b's by means of continued fractions has been discussed in the literature.[24,26]

For values of $(W_y)^{1/2}$ near $\frac{1}{2}l$ or $(W_z)^{1/2}$ near $\frac{1}{2}m$ [i.e., near the singular points of the determinant $\square(0)$], the α's differ considerably from the values $(W_y)^{1/2}$ and $(W_z)^{1/2}$ and for certain ranges become complex. In crystals, the values of $(W_y)^{1/2}$ and $(W_z)^{1/2}$ for which any of the α's becomes complex are not allowed; in these cases the wave function contains a real exponential factor, which becomes infinite at plus or minus infinity. On the contour map of Fig. 5 between α_y^2 as a function of A_y and W_y, shaded areas represent where α_y is complex.[24] Similar contour maps can be drawn for the z direction also. It is to be noticed that these areas are larger, the larger A is, and are smaller, the larger W is.

Having obtained the solution in y and z directions, it remains to solve Eq. (A4) to get the solution in the x direction. A new independent variable η is defined by

$$\eta = (2m/\hbar^2)^{1/3}(B+F)^{-2/3}[A + (B+F)x + a_x] \,. \tag{A17}$$

Equation (A4) then becomes

$$d_2\psi_x/d\eta^2 - \eta\psi_x = 0 \,. \tag{A18}$$

The solution to (A18) may generally be written as

$$\psi_x = a_i \,\mathrm{Ai}(\eta) + b_i \,\mathrm{Bi}(\eta) \,, \tag{A19}$$

where Ai and Bi are Airy functions.

Bi is an exponentially increasing function, and Ai is an exponentially decreasing function. Physically, the tail of the wave function in the region outside the surface must be a rapidly decreasing function; therefore, the solution (A19) reduces to

$$\psi_x = a_i \,\mathrm{Ai}(\eta) \,. \tag{A20}$$

Thus, a particular solution outside the metal surface is given by

$$\psi = N_c e^{i(\alpha_y py + \alpha_z qz)} \left(\sum_{l,m=-\infty}^{\infty} B_{lm} e^{i(lpy + mqz)} \right) \mathrm{Ai}(\eta) \,, \tag{A21}$$

where N_c is some constant.

The most general solution of Eq. (A1) is then given by a series of the form

$$\psi(\vec{k}) = \sum_{r,s} F_{rs} \exp\{i[(\alpha_y + r)py + (\alpha_z + s)qz]\} \times \left(\sum_{lm} B_{lm}(r,s)\, e^{i[lpy + mqz]} \right) \mathrm{Ai}(\eta_{rs}) \,, \tag{A22}$$

where

$$B_{lm}(r,s) = b_{y,l}(\alpha_y + r)\, b_{z,m}(\alpha_z + s) \tag{A23}$$

and

$$\eta_{rs} = (2m/\hbar^2)^{1/3}(B+F)^{-2/3}[A + (B+F)x + a_x(r,s)] \,. \tag{A24}$$

Since both the wave function and its normal derivative must be continuous at the crystal surface,

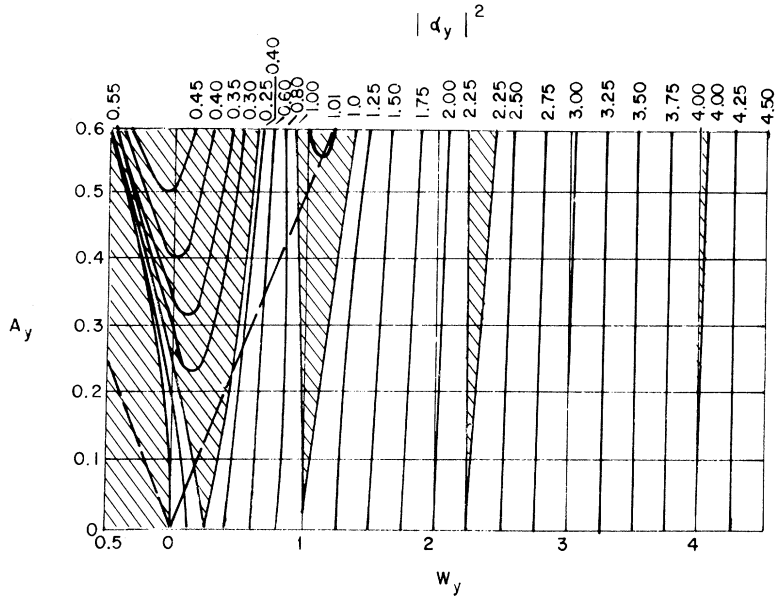

FIG. 5. Values of α_y^2 as a function of A_y and W_y. Shaded portions represent areas where α_y is complex (Ref. 24).

we must take

$$\alpha_y = k_y/p \quad \text{and} \quad \alpha_z = k_z/q \ . \tag{A25}$$

It has been shown in the literature that the α's are the solution of the continued-fraction equation[24,26]

$$D_0 = \frac{1}{D_1} - \frac{A}{D_2} - \frac{A}{D_3} - \cdots + \frac{1}{D_{-1}} - \frac{A}{D_{-2}} - \cdots \ , \tag{A26}$$

where $$D_n = [(\alpha+n)^2 - W]/A \ . \tag{A27}$$

For computation purposes, it is convenient to define

$$f = \alpha^2 - W \ . \tag{A28}$$

Thus,
$$f = \frac{A^2}{(1+2\alpha)+f} - \frac{A^2}{2(2+2\alpha)+f} - \cdots + \frac{A^2}{(1-2\alpha)+f} - \frac{A^2}{2(2-2\alpha)+f} - \cdots \ . \tag{A29}$$

To find the roots of Eq. (A29) first note that this equation is already expressed in a suitable form for solution by means of an iteration process with f regarded as an unknown. Such an iteration procedure was programmed on the University of Pennsylvania 360/75 computer, and we obtained f_y and f_z to an accuracy of four significant figures. It has been shown in the literature[26] that this iteration process converges in an alternating fashion. The number of iterations required to solve (A29) was extremely large. This was due to the poor convergence for some values of α and A. To reduce the number of iterations in the solution of Eq. (A29), two cases were differentiated[26]: (a) fast convergence f'_{n+1} contained within the interval (f_n, f_{n+2}), (b) slow convergence f'_{n+1} outside the interval (f_n, f_{n+2}), where f_{n+1} is the result of the nth iteration, using f_n as the trial value and f'_{n+1} as the arithmetic mean of f_{n+1} and f_n. In the case of slow convergence, f'_{n+1} was used as the next trial value for the $(n+2)$ iteration. Figure 6 represents the function f, which, as explained, represents the difference between α^2 and W and is thus a measure by which the characteristic exponent differs from the free-electron case. The characteristic exponent α differs considerably from W near the singular points of Hill's determinant. Our values of f compare favorably with those available in the literature.[26] Having obtained the

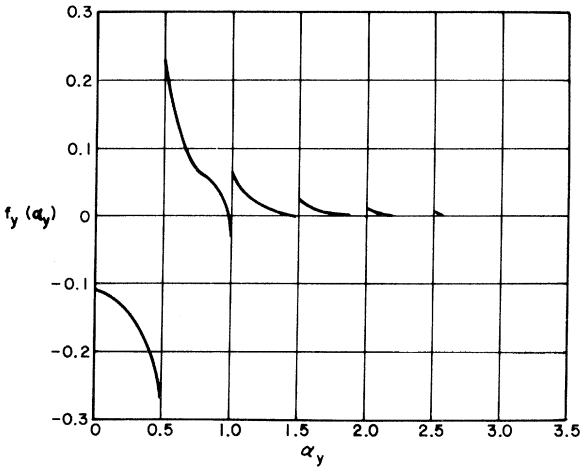

FIG. 6. Values of $f(\alpha_y)$ for real values of α_y for $A_y = \frac{1}{4}$.

function f, we may easily obtain the separation constant W. The Fourier coefficients $b_{y,l}(\alpha_y)$ and $b_{z,m}(\alpha_z)$ were then determined by solving the continued-fraction equations.

The basic recursion formula for b's as shown in the literature[26,27] is given by

$$[(\alpha+n)^2 - W]\, b_n - A b_{n+1} - A b_{n-1} = 0 \ . \qquad \text{(A30)}$$

This is a three-term recursion formula for α and b_n's. Equation (A30) can be written

$$\frac{b_n}{b_{n-1}} = \frac{A}{(\alpha+n)^2 - W - A(b_{n+1}/b_n)} \qquad \text{(A31)}$$

and, similarly,

$$\frac{b_n}{b_{n+1}} = \frac{A}{(\alpha+n)^2 - W - A(b_{n-1}/b_n)} \ . \qquad \text{(A32)}$$

Equation (A31) shows that when n is large and positive, b_n/b_{n-1} is small and approaches zero proportional to $1/n^2$ if the next ratio b_{n+1}/b_n also approaches zero for large n, because in that case for large enough n, the term $(\alpha+n)^2$ is much larger than all the other terms in the denominator and $b_n/b_{n-1} \to A/n^2$. Likewise, $b_n/b_{n+1} \to A/n^2$. Thus, (A31) and (A32) satisfy the convergence test. Values of $b_{y,l}$ and $b_{z,m}$ were computed in terms of $b_{y,0}$ and $b_{z,0}$, and the values of $b_{y,0}$ and $b_{z,0}$ are adjusted so that

$$\sum_l b_{y,l}^2 = 1 \quad \text{and} \quad \sum_m b_{z,m}^2 = 1$$

for normalization purposes. A computer program was developed for this purpose. It was observed, as expected, that as l and m increase, the coefficients $b_{y,\pm l}$ and $b_{z,\pm m}$ decrease rapidly. In fact, only the terms up to l and m equal to 5 were significant. Figure 7, adopted from Morse,[24] also confirms this conclusion. The separation constants W_y and W_z are given by

$$W_y(\alpha_y) = \alpha_y^2 + f_y \qquad \text{(A33)}$$

and

$$W_z(\alpha_z) = \alpha_z^2 + f_z \ . \qquad \text{(A34)}$$

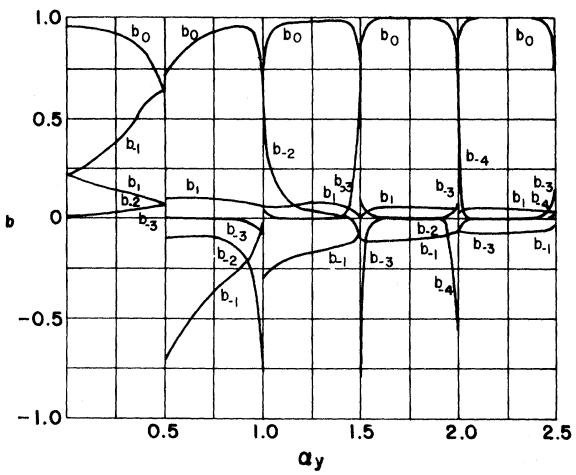

FIG. 7. Values of the Fourier coefficients $b_l(\alpha_y)$ for real values of α_y, for $A_y = \frac{1}{4}$. Coefficients not shown in this figure are negligibly small (Ref. 24).

$a_x(r,s)$ will then be given by

$$a_x(r,s) = (\hbar^2 p^2/2m)\,[(\alpha_y+r)^2 + f_y(r)\,] + (\hbar^2 q^2/2m)\,[(\alpha_z+s)^2 + f_z(s)\,] \ . \qquad \text{(A35)}$$

Boundary conditions require the wave function and its normal derivative to be continuous across the crystal surface. Thus,

$$[\psi(x'>0)]_{x=C_y(\cos py)+C_z(\cos qz)} = [\psi(x'<0)]_{x=C_y(\cos py)+C_z(\cos qz)} \qquad \text{(A36)}$$

and

$$[\psi'(x'>0)]_{x=C_y(\cos py)+C_z(\cos qz)} = [\psi'(x'<0)]_{x=C_y(\cos py)+C_z(\cos qz)} \ . \qquad \text{(A37)}$$

The coefficients A_{rl} and F_{rs} are determined by the standard procedure of changing the variables y and z in the resulting equation by $py = \theta$ and $qz = \phi$, multiplying by $\exp\{-i[(k_y/p)\theta + n\theta]\}$ and $\exp[-i(k_z\phi/q + m\phi)]$, and integrating the resulting equations over θ and ϕ from $-\pi$ to π. Condition (A36) thus leads to simultaneous equations of the form

$$(i)^{n+m} 4\pi^2 \left(J_n(k_x C_y) J_m(k_x C_z) + \sum_{r,l} A_{rl} J_{r-n}(k_{xrl} C_y) J_{l-m}(k_{xrl} C_z)(-i)^{r+l} \right) = \sum_{r,s} F_{rs} H_{rsnm} \ , \qquad \text{(A38)}$$

where

$$H_{rsnm} = \int_{-\pi}^{\pi}\int_{-\pi}^{\pi} e^{i(r-n)\theta} e^{i(s-m)\phi} \sum_{l,t} B_{lt}(r,s)\, e^{i(l\theta + t\phi)}\, \mathrm{Ai}(\eta''_{rs})\, d\theta\, d\phi \ , \qquad \text{(A39)}$$

and

$$\eta''_{rs} = (2m/\hbar^2)^{1/3}(B+F)^{-2/3}\,\{A + (B+F)(C_y \cos py + C_z \cos qz) + (\hbar^2 p^2/2m)\,[(\alpha_y+r)^2 + f_y(\alpha_y, r)\,] + (\hbar^2 q^2/2m)\,[(\alpha_z+s)^2 + f_z(\alpha_z, s)\,]\,\} \ . \qquad \text{(A40)}$$

Equation (A37) will lead to the simultaneous equations of the form

$$4\pi^2(i)^{n+m}\left\{iJ_n(k_xC_y)J_m(k_xC_z)\left(k_x-\frac{pk_yn}{k_x}-\frac{qk_zm}{k_x}\right)+\sum_{r,l}A_{rl}(-i)^{r+l+1}J_{r-n}(k_{xrl}C_y)J_{l-m}(k_{xrl}C_z)\right.$$
$$\left.\times\left[k_{xrl}+\frac{(r-n)p(k_y+rp)}{k_{xrl}}+\frac{(l-m)q(k_z+lq)}{k_{xrl}}\right]\right\}=\sum_{r,s}F_{rs}G_{rsnm}\,, \tag{A41}$$

where

$$G_{rsnm}=\int_{-\pi}^{\pi}\int_{-\pi}^{\pi}\left[e^{i[(r-n)\theta+(s-m)\phi]}\left(\sum_{l,t}B_{lt}e^{i(l\theta+t\phi)}\right)\mathrm{Ai}'(\eta_{rs}'')\,U'+iC_yp^2\sin\theta\left(\sum_{l,t}B_{lt}(\alpha_y+r+l)e^{i(l\theta+t\phi)}\right)\right.$$
$$\left.\times\mathrm{Ai}(\eta_{rs}'')+iC_zq^2\sin\phi\left(\sum_{l,t}B_{lt}(\alpha_z+s+t)\,e^{i(l\theta+t\phi)}\right)\mathrm{Ai}(\eta_{rs}'')\right]d\theta\,d\phi\ . \tag{A42}$$

J_i is the Bessel function of ith order and Ai′ represents the derivative of the Airy function with respect to its arguments. U' is given by

$$U'=(2m/\hbar^2)^{1/3}(B+F)^{1/3}\ . \tag{A43}$$

m and n can take all integral values from $-\infty$ to ∞. Equations (A38) and (A41) comprise a set of $2K$ simultaneous equations. In fact, each of Eqs. (A38) and (A41) comprises a set of infinite simultaneous equations. These two sets of infinite simultaneous equations are enough to determine all F's and A's. To a first approximation we can solve these equations analytically, but to get the amplitudes of secondary waves these equations can only be solved numerically. A suitable computer program was developed for this purpose. We used Simpson's rule in two dimensions for evaluating the integrals appearing in (A39) and (A42). To reduce the time spent on the computer, we took into account that the transmitted waves represented by the higher indices of r and s were not significant. Because of the presence of Airy functions in the transmitted waves, the terms involving higher values of r and s drop very sharply. This has a direct physical explanation, namely, out of all the possible transmitted waves, only the primary transmitted beam represented by F_{00} and the secondary beams with r and s in the neighborhood of zero are important. A computer program available in the University of Pennsylvania Computer Library, with an accuracy of five significant figures, was used to solve the simultaneous equations with complex coefficients (A38) and (A41).

*Part of work supported by NASA Grant No. NSG 316 to the Institute for Direct Energy Conversion, University of Pennsylvania, Philadelphia, Pa.

†Paper based in part on a dissertation submitted by Satya P. Sharma in partial fulfillment of the requirements for the Ph.D. degree at the University of Pennsylvania, Philadelphia, Pa. Present address: Bell Telephone Laboratories, Columbus, Ohio 43213.

[1]E. W. Müller, in *Advances in Electronics and Electron Physics* (Academic, New York, 1960), pp. 83–179.
[2]R. Gomer, *Field Emission and Field Ionization* (Harvard U. P., Cambridge, Mass., 1961).
[3]T. T. Tsong and E. W. Müller, J. Chem. Phys. 41, 3279 (1964).
[4]A. J. Jason, Phys. Rev. 156, 266 (1967).
[5]M. E. Alferieff and C. B. Duke, J. Chem. Phys. 46, 938 (1967).
[6]S. J. Fonash and G. L. Schrenk, Phys. Rev. 180, 649 (1969).
[7]D. S. Boudreaux and P. H. Cutler, Phys. Rev. 149, 170 (1966).
[8]D. G. Brandon, Phil. Mag. 7, 1003 (1962).
[9]Z. Knor and E. W. Müller, Surface Sci. 10, 21 (1968).
[10]C. Herring, *Metal Interfaces* (American Society for Metals, Cleveland, Ohio, 1952), pp. 1–19.
[11]R. Smoluchowski, Phys. Rev. 60, 661 (1941).
[12]J. Bardeen, Phys. Rev. 49, 653 (1936).
[13]C. H. Kelly, thesis, Polytechnic Institute of Brooklyn, 1954 (unpublished).
[14]C. B. Duke, J. Vacuum Sci. Technol. 6, 152 (1969).
[15]J. R. Smith, Phys. Rev. 181, 522 (1969).
[16]N. D. Lang, Solid State Commun. 7, 1047 (1969).
[17]P. H. Cutler and J. C. Davis, Surface Sci. 1, 194 (1964).
[18]T. Loucks and P. H. Cutler, J. Phys. Chem. Solids 25, 105 (1964).
[19]B. A. Lippmann, Phys. Rev. 102, 264 (1956).
[20]B. A. Lippmann and J. Schwinger, Phys. Rev. 79, 469 (1950).
[21]J. C. Maxwell, *A Treatise on Electricity and Magnetism* (Dover, New York, 1962).
[22]J. Callaway, *Energy Band Theory* (Academic, New York, 1964), pp. 37–38, 279.
[23]H. R. Hasse, Proc. Cambridge Phil. Soc. 26, 542 (1930).
[24]P. M. Morse, Phys. Rev. 35, 1310 (1930).
[25]S. P. Sharma and G. L. Schrenk, in Proceedings of Sixteenth Field Emission Symposium, Pittsburgh, Pa. (unpublished).
[26]T. Tamir, Math. Comp. 16, 77 (1962).
[27]P. M. Morse and H. Feshbach, *Methods of Theoretical Physics* (McGraw-Hill, New York, 1953), Part 2.